IOP Publishing Journal of Optics
J. Opt. 21 (2019) 065605 (20pp) https://doi.org/10.1088/2040-8986/ab1d2f

Dynamic characteristics of nematic liquid crystal variable retarders investigated by a high-speed polarimetry

Song Zhang, Chao Chen, Hao Jiang[1], Honggang Gu, Xiuguo Chen, Chuanwei Zhang and Shiyuan Liu

State Key Laboratory of Digital Manufacturing Equipment and Technology, Huazhong University of Science and Technology, Wuhan 430074, People's Republic of China

E-mail: hjiang@hust.edu.cn and shyliu@hust.edu.cn

Received 5 February 2019, revised 10 April 2019
Accepted for publication 26 April 2019
Published 23 May 2019

Abstract

Liquid crystal variable retarders (LCVRs) have been widely used as a transmissive element with electrically tunable optical phase retardance in polarimetric optical systems. Since the responsive characteristics of the LCVRs depend on the modulation processes, accurately and rapidly characterizing LCVRs is of great significance for the performance improvement of the optical system with LCVRs. Firstly, we proposed a Mueller matrix based model to characterize an LCVRs with considerations of both linear birefringence (LB) and circular birefringence (CB), with which the LCVRs is described by several driving voltage-dependent optical parameters such as retardance, azimuth, relative transmittance and optical rotation angle. The experimental results show that the Mueller matrices of the LCVRs measured by a commercial Mueller matrix ellipsometer are consistently fitted by the proposed method, and the improvement of the proposed characterization method can be read from the 15 times reduced average residual errors of the reconstructed Muller matrix compared to the matrix reconstructed with the conventional characterization methods. Through several typical dynamic measurement experiments using a high-speed Stokes polarimeter with a temporal resolution of several nanoseconds, we demonstrated the driving-voltage-dependence of these optical parameters as well as the existence of both LB, CB and depolarization properties in the LCVRs modulation processes. Based on the analysis of the extracted optical parameters, we have obtained the continuous modulation characteristics and step response characteristics of LCVRs. Additionally, a comparison between the Mueller matrices of air measured with the proposed and conventional characterization method has been carried out to demonstrate the fidelity of the proposed method as well.

Keywords: liquid crystal variable retarders (LCVRs), dynamic modulation, characterization, Stokes polarimeter

(Some figures may appear in colour only in the online journal)

1. Introduction

Nowadays, polarimetry is an indispensable technique across many fields, such as astronomy [1–4], remote sensing [5–7] and material characterization [8–11]. Nematic liquid crystal variable retarders (LCVRs) have been widely used as a transmissive element with electrically tunable optical phase retardance in the variable retardance polarimetry [12–15] and other polarimetric optical systems [16, 17]. Since the characteristics of the LCVRs depend on the modulation processes, dynamic characterization of the LCVRs modulation process is of great significance for the performance improvement in both accuracy and temporal resolution of an optical system with LCVRs.

[1] Author to whom any correspondence should be addressed.

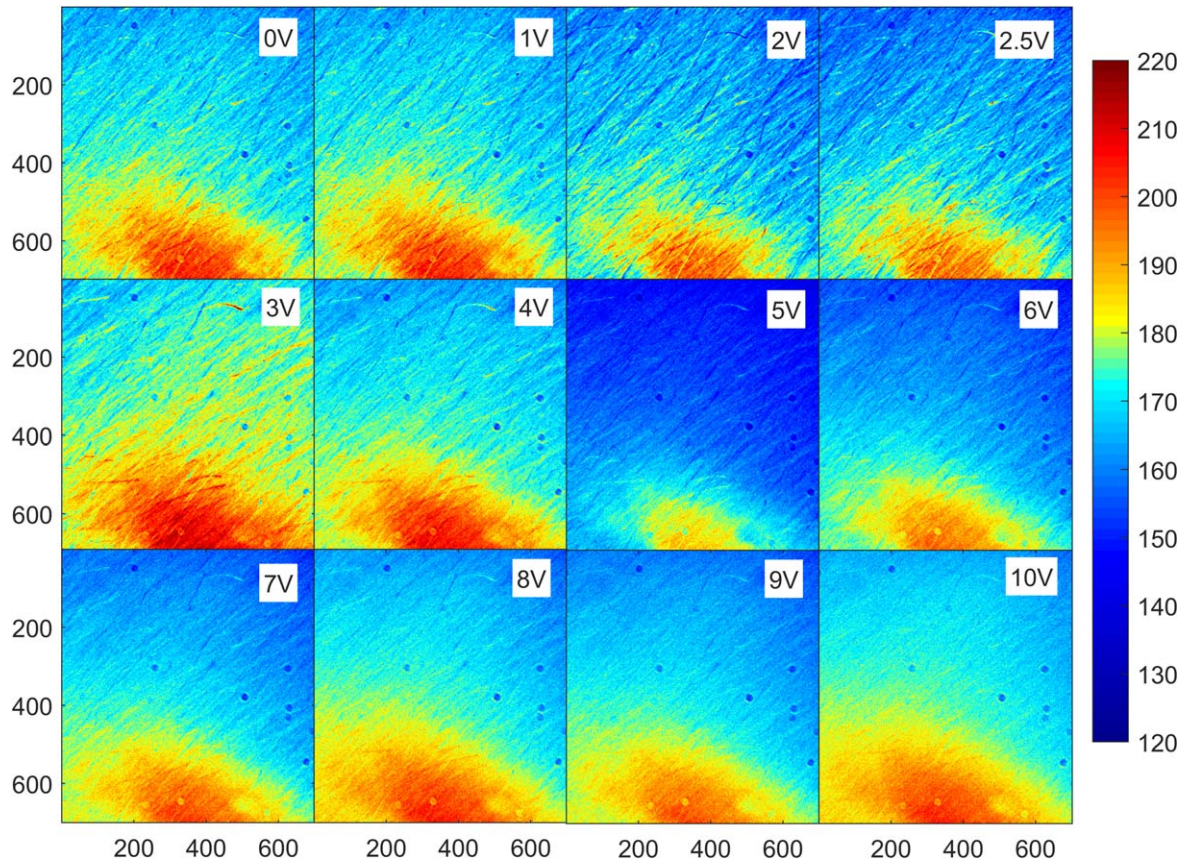

Figure 1. Light intensity distribution of the LCVRs at different driving voltage observed by a metallographic microscope: The axis represents the number of pixels, and the value of the color bar represent the intensity of light detected by the CCD; the experimental configuration is Eyepiece: PL 10×/22 (Field No. 20 mm); Objectives: 5×/0.15 (NA).

In recent years, many researchers have been engaged in characterizing the electro-optic and time response characteristics of the LCVRs. Hilfiker *et al* studied the linear birefringence (LB) property and the driving voltage dependence of the retardance for the LCVRs [18–21]. Terrier *et al* additionally considered the driving voltage dependence of the azimuth based on previous characterization methods with the objective to improve the performance of an imaging spectrometer [22]. López-Téllez *et al* characterized the optical polarization properties of the LCVRs with consideration of LB, linear diattenuation (LD) and depolarization, but there is little discussion about the dynamic characteristics of LCVRs [23]. Heredero *et al* investigated the correlation between the response times and temperature under different applied voltage changes [24]. Ma *et al* observed the directions of liquid crystal molecular in real-time with a snapshot polarimeter, and found that the LC molecular dynamics are affected by the impurity ions in the LC cells [25]. Due to the absence of the appropriate tools and accurate characterization model, the systematic study on the dynamic responsive characteristics of LCVRs are rarely explored. Besides, in most of the existing studies on LCVRs, the circular birefringence (CB) property is usually ignored, which may degrade the accuracy of the characterization [26]. Missing of the voltage-dependent optical properties of LCVRs will consequently limit their applications in the optical system with emphasis on the accuracy as well as high temporal resolution [22, 27]. It is highly desirable that there is a method that can characterize the various properties of LCVRs during the rapid dynamic modulation processes accurately.

At present, the fastest modulation frequency of LCVRs can be several kilohertz [28]. To completely capture the details of the dynamic modulation process, the time resolution required by the measurement must be at least microsecond or even sub-microsecond. The highest time resolution of the existing polarimeter is about sub-millisecond [29]. Therefore, the self-developed Stokes polarimeter which has a time resolution of several nanoseconds, and can measure all the Stokes vectors in one measurement [30, 31] shows advantages for the study of the rapid modulation processes of LCVRs.

In this work, a Mueller matrix based model to characterize an LCVRs with considerations of both LB and CB is proposed at first. In the proposed characterization model, the LCVRs are described by the voltage-dependent optical parameters of relative transmittance A, retardance δ, azimuth β and optical rotation angle γ. The improvement can be read from the decreased residual errors, which is defined as the deviations from the Mueller matrices reconstructed by the proposed model and by the conventional model to the values measured by the commercial Mueller matrix ellipsometer (MME). Then, the self-developed Stokes polarimeter has been applied for investigating the modulation characteristics of LCVRs through several typical dynamic measurement experiments. We have demonstrated the driving-voltage-

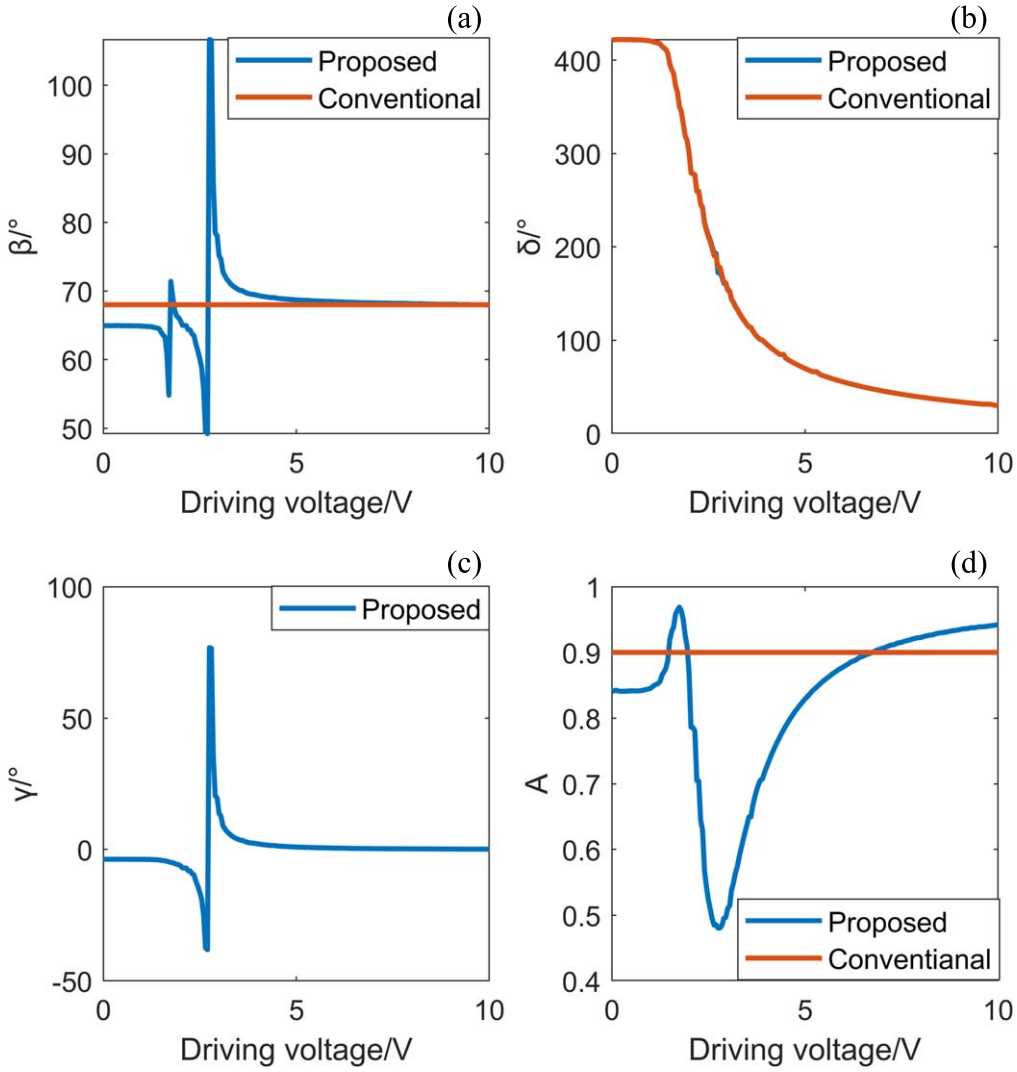

Figure 2. Electro-optic characteristic parameters of LCVRs characterized with proposed and conventional characterization method: (a) azimuth β of LCVRs versus driving voltage; (b) retardance δ of LCVRs versus driving voltage; (c) optical rotation angle γ of LCVRs versus driving voltage; (d) relative transmittance A of LCVRs versus driving voltage.

dependence of these optical parameters as well as the existence of both LB, CB and depolarization properties in the LCVRs modulation processes. Based on the analysis of the extracted optical parameters, we have obtained the continuous modulation characteristics and step response characteristics of LCVRs. Additionally, the average residual error less than 1% on the measured Mueller matrix of the air based on the dynamic responsive characteristics of LCVRs demonstrated the fidelity of the proposed method as well.

2. Characterization of the LCVRs based on Mueller matrix

Typical nematic LCVRs modulate the retardance electrically by changing the effective birefringence of the nematic liquid crystal materials. The LCVRs are constructed by two optically flat fused silica windows coated with a transparent conductive coating which is made of indium tin oxide (ITO). Then, the ITO layer is covered by a thin dielectric layer which is the molecular alignment layer [32]. Finally, the two windows are assembled a few microns apart to create a cavity that will be filled with birefringent nematic liquid crystal material.

The principle of the retardance modulation of the LCVRs is that the orientation of liquid crystal molecules (LCMs) changes regularly with external voltage applied. With no external voltage applied, the long axes of the molecules nominally lie parallel to the glass substrates with a naturally twisted orientation, and the maximum retardation is achieved. With an increasing applied voltage, the molecules tip further causing a reduction in the effective retardance until tipping perpendicular to the substrates to achieve a minimum retardance while keeping the twisted orientation. It should be noted that there is a residual retardance due to the fixed molecules pined at the alignment layer [33].

A metallographic polarizing microscope (Ningbo Sunny instrument CO. LTD, BH200M) equipped with a pair of fast axis orthogonal polarizers has been applied to observe the state of the LCMs in the LCVRs (Meadowlark Optics, LVR-100) at different driving voltages for a better understanding of the modulation characteristics. The light intensity distribution of the LCVRs at

different driving voltage are shown in figure 1. It can be observed that the fibrous LCMs with different colors are in different orientations under the metallographic microscope. Besides, the fibrous LCMs gradually disappear as the driving voltage increases, corresponding to the processes of LCMs rotating from parallel and perpendicular to the glass substrates, respectively. The experimental phenomena are consistent with the changes in LCMs during the modulation processes mentioned above. Meanwhile, it is well known that there is a CB property in the LCMs [34], and combined with the change law of the fibrous LCMs and the variation of light intensity distribution in the driving voltage range of 2–3 V, it is speculated that the phenomenon may be due to the strongest CB properties of the LCVRs in such driving voltage range. Besides, the LCMs are unevenly distributed in the LCVRs according to the light intensity distribution.

According to the observations under the metallographic microscope, it has been confirmed the LCVRs exhibit both LB and CB properties during the modulation processes. It is worth emphasizing that there is little LD property in the modulation processes of the LCVRs [23]. In order to simplify the calibration model, the LD property is not considered in the characterization experiments. Therefore, the characterization of the LCVRs using Mueller matrix described by relative transmittance A, optical rotation angle γ, azimuth β and retardance δ can be expressed as

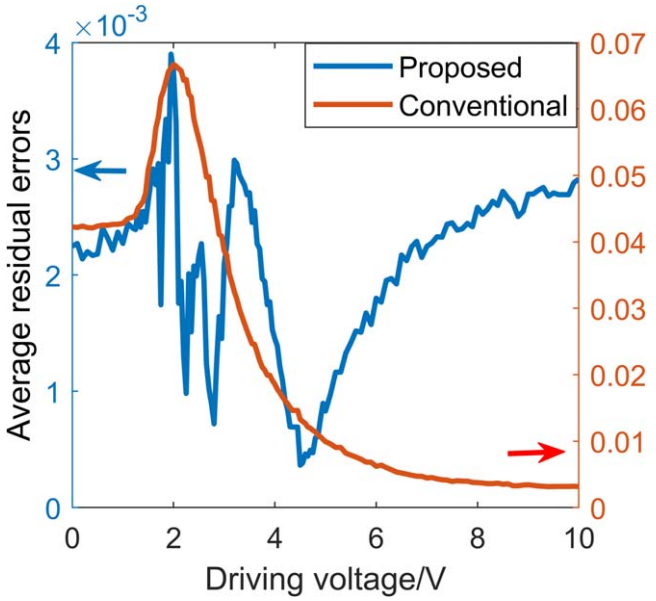

Figure 3. The average residual errors of the Mueller matrix elements achieved by the proposed and conventional characterization models.

Different from the conventional characterization method where only the LB property is taken into consideration [38–40], the proposed method introduces the CB property and the voltage dependence of the optical parameters. As an example, we use a commercial broadband MME (ME-L, Wuhan Eoptics Technology Co, Ltd) to measure the Mueller matrices of the LCVRs under a series of discrete constant driving voltages. Then the Muller matrices of the LCVRs will be fitted with the least squares fitting algorithm by both the proposed and the conventional characterization methods, and the comparison of the extracted optical parameters has been shown in figure 2.

In the conventional characterization method, other optical parameters except the retardance are driving voltage independent. However, as shown in figure 2, all the optical parameters of the LCVRs change with the driving voltage. It should be noted that the extracted retardance achieved by both

$$\mathbf{M}_{\mathrm{LCVRs}}(A,\,\alpha,\,\beta,\,\delta) = A\cdot\mathbf{M}_{\mathrm{CB}}(\gamma)\cdot\mathbf{M}_{\mathrm{LB}}(\beta,\,\delta)$$
$$= A\cdot\begin{pmatrix} 1 & 0 & 0 & 0 \\ 0 & \cos(2\beta)\cos(2\alpha) - \sin(2\beta)\sin(2\alpha)\cos(\delta) & \sin(2\beta)\cos(2\alpha) + \cos(2\beta)\sin(2\alpha)\cos(\delta) & \sin(2\alpha)\sin(\delta) \\ 0 & -\cos(2\beta)\sin(2\alpha) - \sin(2\beta)\cos(2\alpha)\cos(\delta) & \cos(2\beta)\cos(2\alpha)\cos(\delta) - \sin(2\beta)\sin(2\alpha) & \cos(2\alpha)\sin(\delta) \\ 0 & \sin(2\beta)\sin(\delta) & -\cos(2\beta)\sin(\delta) & \cos(\delta) \end{pmatrix}, \quad (1)$$

where $\alpha = \gamma - \beta$. It is worth noting that the order $\mathbf{M}_{\mathrm{CB}}(\gamma)\cdot\mathbf{M}_{\mathrm{LB}}(\beta,\delta)$ is chosen because the azimuth calculated by the order is closer to the azimuth set in the experiment. The Mueller matrix of a device with LB properties such as a wave plate or a retarder with a fast axis azimuth of β and a retardance δ [35] can be expressed as

$$\mathbf{M}_{\mathrm{LB}} = \begin{pmatrix} 1 & 0 & 0 & 0 \\ 0 & \cos(4\beta)\sin(\delta/2)^2 + \cos(\delta/2)^2 & \sin(4\beta)\sin(\delta/2)^2 & -\sin(2\beta)\sin(\delta) \\ 0 & -\sin(4\beta)\sin(\delta/2)^2 & -\cos(4\beta)\sin(\delta/2)^2 + \cos(\delta/2)^2 & \cos(2\beta)\sin(\delta) \\ 0 & \sin(2\beta)\sin(\delta) & \cos(2\beta)\sin(\delta) & \cos(\delta) \end{pmatrix}, \quad (2)$$

and the Mueller matrix for a device with CB properties, such as an optically active material with an optical rotation angle γ [36, 37], can be written as equation (3)

$$\mathbf{M}_{\mathrm{CB}} = \begin{pmatrix} 1 & 0 & 0 & 0 \\ 0 & \cos(2\gamma) & \sin(2\gamma) & 0 \\ 0 & -\sin(2\gamma) & \cos(2\gamma) & 0 \\ 0 & 0 & 0 & 1 \end{pmatrix}. \quad (3)$$

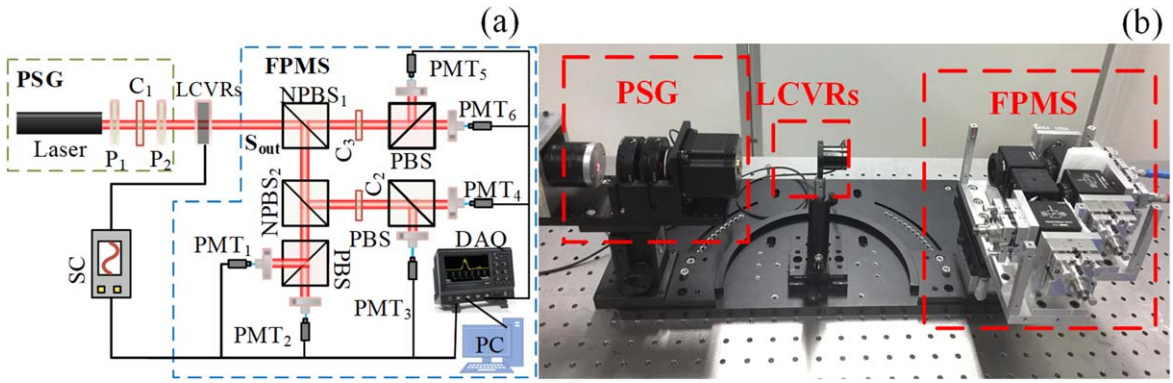

Figure 4. A six-channel Stokes polarimeter: (a) light path diagram: P_1 and P_2—polarizers; C_1 and C_3—quart-wave plate; S—LCVRs; C_2—half-wave plate; $NPBS_1$—70:30 (R:T) non-polarization beam splitter; $NPBS_2$—50:50 (R:T) non-polarization beam splitter; PBS—polarization beam splitter; DAQ—oscilloscope; PC—personal computer; SC—signal controller; PMT_i—photomultiplier tube. (b) Self-developed Stokes polarimeter prototype.

characterization models are identical as shown in figure 2(b), which is because the retardance share the same expression in different models. It can be observed that the optical rotation angle of the LCVRs achieved by the proposed characterization model are not 0 when the driving voltage is in the range of 2.3–3.1 V as shown in figure 2(c). Meanwhile, the voltage-dependent azimuth shows large differences in such interval as shown in figure 2(a). As shown in figure 2(d), the relative transmittance will fluctuate drastically with the increase of driving voltage instead of remaining unchanged.

Then, we use the optical parameters extracted by different characterization methods to reconstruct the Muller matrices of the LCVRs respectively. After that, the reconstructed Mueller matrices will be compared based on the Muller matrices measured by the MME. If the residual errors and average residual errors of the Mueller matrix elements are defined as equations (4) and (5), respectively, the average residual errors of the Mueller elements of the proposed and conventional characterization methods are shown in figure 3.

$$\Delta m_{ij} = m_{ij}^{\mathrm{c}} - m_{ij}^{\mathrm{m}}, \tag{4}$$

where m_{cij} and m_{mij} $(i, j = 0, 1, 2, 3)$ are the ith row and jth column elements of the reconstructed and the measured Mueller matrices, respectively

$$Er_{\mathrm{ave}} = \sqrt{\frac{\sum_{i=0}^{3}\sum_{j=0}^{3}\Delta m_{ij}^{2}}{16}}. \tag{5}$$

It can be observed that the average residual errors of Mueller matrix elements from the proposed characterization model are significantly reduced about 15 times compared with the conventional characterization model. Both the reduced residual errors and more detailed transit processes captured can be used to show the improvement of the proposed characterization model.

3. Instrument and experiment preparation

The instrument for measuring the dynamic modulation processes of the LCVRs is a self-developed Stokes polarimeter with six parallel detection channels. As schematically shown in figure (4), the Stokes polarimeter is based on the spatial division of amplitude, and consists of three parts: a polarization state generator (PSG), a sample stage and a fast polarization measurement system (FPMS). The light source is a 5 mW Red (632.8 nm) He–Ne Laser (THORLABS). The PSG can output the polarized light of any polarization state. Meanwhile, the FPMS can detect all the Stokes parameters of the probing light in several nanoseconds. The polarimeter is mounted on a rotatable base so that it can be used in both transmissive mode, and reflective mode with multi-incident angles [30, 31]. The experiments are carried out in a clean room with constant temperature and humidity. Therefore, the influence of the temperature is not considered in our experiments.

The LCVRs used in our experiment are controlled with a 2 KHz square wave output signals in several computer-based methods to simulate various types of modulated signals. The LCVRs is a commercial product that have good stability and repeatability of the same modulation processes. Due to the strong coupling between the optical rotation angel and the azimuth, the optical parameters of the same dynamic modulation processes are extracted by using two sets of measurement configurations respectively in order to simplify the data analysis. First, the retardance of the LCVRs is extracted from Stokes parameters S_3 when the polarization state of the incident light is left-hand circular polarization. Then the value of α can be extracted from $S_2/\sin(\delta)$ or $S_3/\cos(\delta)$, as shown in equation (6). Meanwhile, the azimuth of the LCVRs can be extracted from the $S_3/\sin(\delta)$ when the incident light is a linear polarized light of 45°, as shown in equation (7)

$$\begin{aligned}\mathbf{S}_{\mathrm{out}} &= \mathbf{M}_{\mathrm{LCVRs}} \cdot [1 \;\; 0 \;\; 0 \;\; 1]^{\mathrm{T}} \\ &= \left[1 \;\; \sin(2\alpha)\sin(\delta) \;\; \cos(2\alpha)\sin(\delta) \;\; \cos(\delta)\right]^{\mathrm{T}},\end{aligned} \tag{6}$$

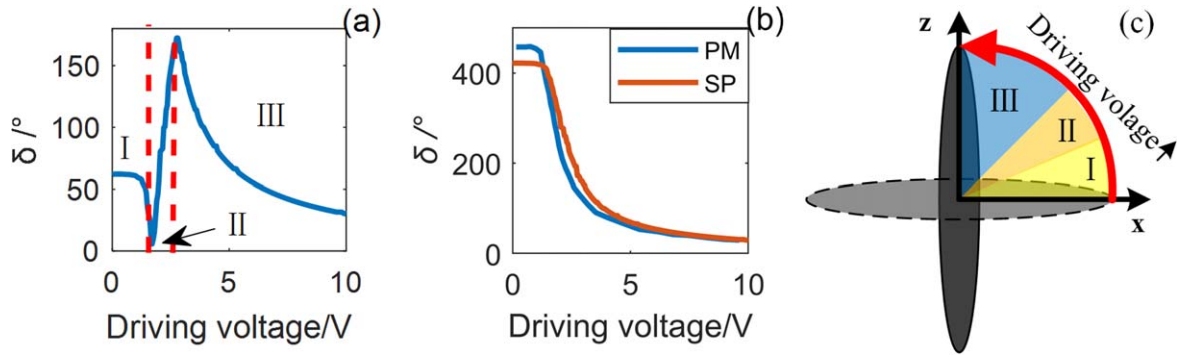

Figure 5. Modulation process of LCVRs in a series of discrete constant driving voltage: (a) retardance of the LCVRs measured by Stokes polarimeter is 'wrapped' into a range from 0° to 180°; (b) 'unwrapped' retardance of the LCVRs measured with Stokes polarimeter and provided by the manufacturer. where 'PM' represents the results provided by the manufacturer; 'SP' represents the results measured by the Stokes polarimeter; (c) segmentation diagram of liquid crystal molecule rotation process, where the *x*-axis direction is parallel to the glass substrates and the *z*-axis direction is perpendicular to the glass substrates.

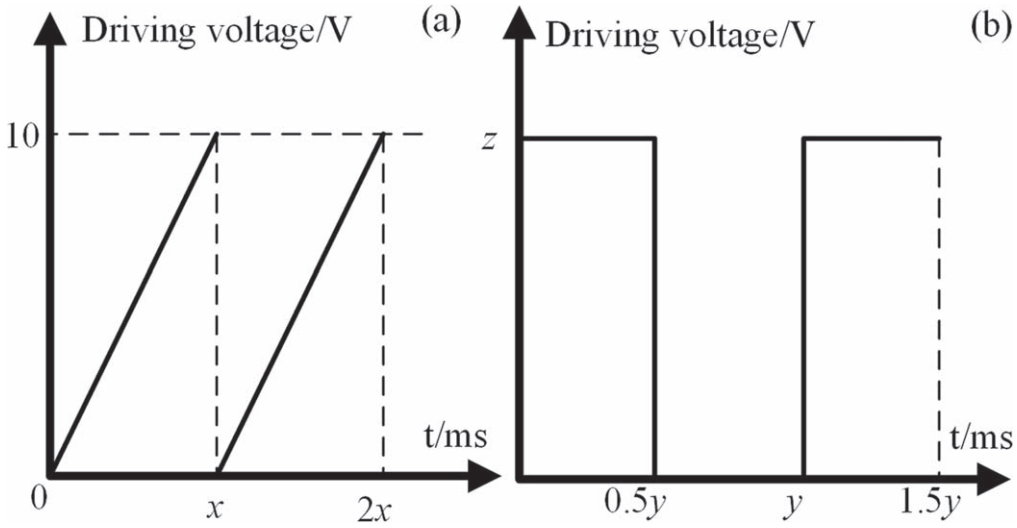

Figure 6. Schematic diagram of modulation signals: (a) sawtooth with modulation periods of x ms (x = 20–20 000), (b) 0–z V (z = 1–10) square wave with modulation periods of y ms (y = 20–20 000).

$$\mathbf{S}_{\text{out}} = \mathbf{M}_{\text{LCVRs}} \cdot [1 \quad 0 \quad 1 \quad 0]^{\text{T}} = \left[1 \quad S_1 \quad S_2 \quad -\cos(2\beta)\sin(\delta)\right]^{\text{T}}. \tag{7}$$

In order to validate the performance of the self-developed Stokes polarimeter and the correctness of the proposed measurement method of the optical parameters, we first use the polarimeter to measure the static modulation process of LCVRs in a series of discrete constant driving voltage. Since only the curve of the retardance against the driving voltage is provided by the manufacturer, a comparison between the measured retardance and manufacturer provided data has been carried out, as shown in figure 5.

As shown in figure 5(a), the retardance measured by the Stokes polarimeter is wrapped into the range from 0° to 180°, so we perform the phase unwrapping procedure [38] to get the actual retardance, as shown in figure 5(b). It is observed that the retardance measured by the Stokes polarimeter is consistent with the results provided by manufacturer in general. However, the threshold voltage of the retardance measured by the polarimeter is slightly larger than the results provided by the manufacturer. When the driving voltage is in the range of 1.5–3.5 V, the retardance of the LCVRs measured by the polarimeter falls faster compared with the results provided the manufacturer. However, the residual retardance achieved is consistent when the driving voltages are beyond 5 V. These subtle differences are mainly caused by the different measurement conditions and methods.

In order to establish the relationship between the measured modulation results and the state of the LCMs and to facilitate subsequent data analysis procedure, the subsequent results will not be 'unwrapped' into the full variation range of the retardance as shown in figure 5(b). Then, the retardance variations can be divided into three regions: I startup region, II fast transit region and III stable region, which correspond to the LCM rotation status, as shown in figure 5(c).

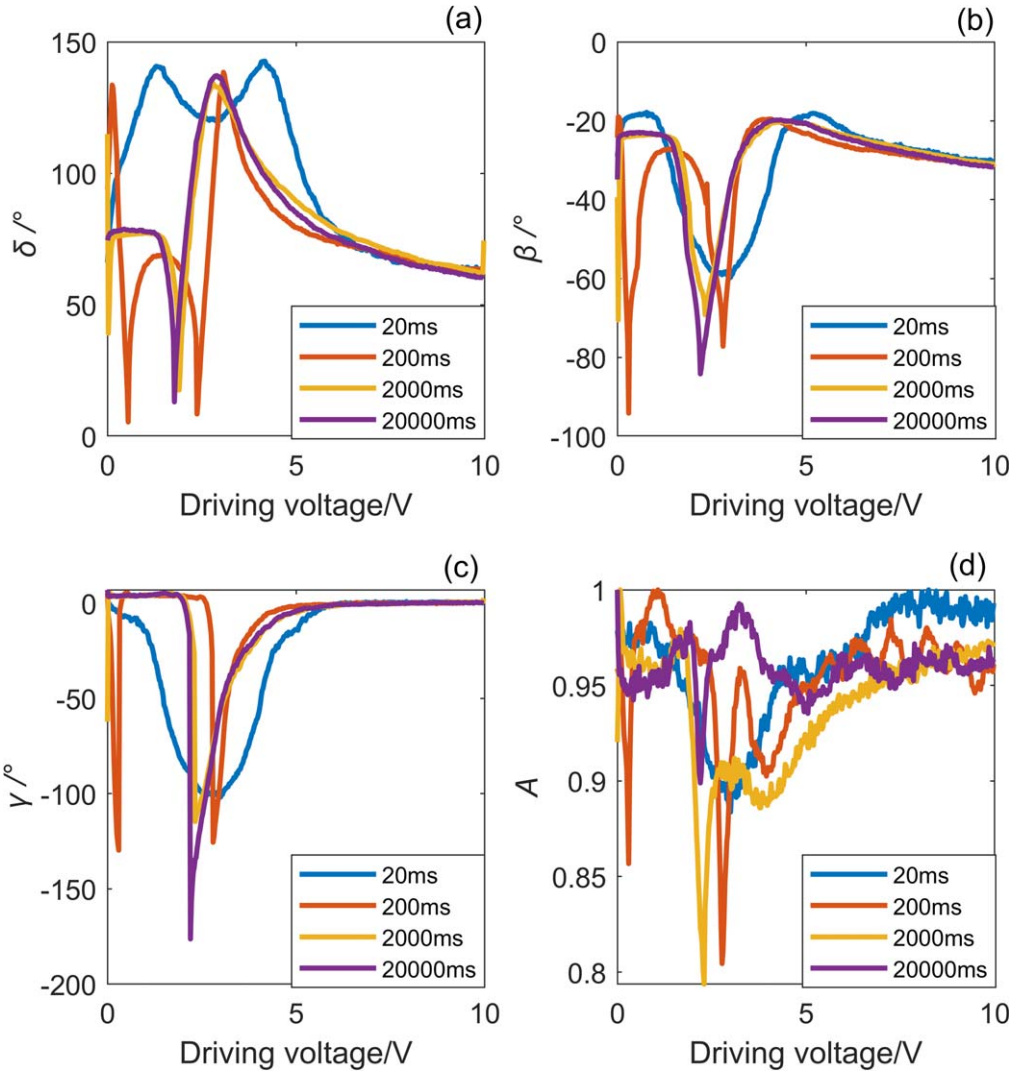

Figure 7. Optical parameters of the LCVRs modulated by sawtooth signals of different periods of x ms (x = 20–20 000). In order to more clearly and concisely show the evolution process, only the results of 20, 200, 2000, 20 000 ms are given in the figure.

4. Dynamic measurement experiments

In this section, the dynamic responsive characteristics of the LCVRs during several typical dynamic modulation processes are investigated by the self-developed Stokes polarimeter. The sawtooth signals of various modulation periods as shown in figure 6(a), and the square wave signals with variable amplitudes and periods as shown in figure 6(b), are used as modulation signals for the dynamic response characteristics study.

4.1. Modulated by sawtooth signals with different periods

In this part, we use the sawtooth signals with different periods as applied voltage to explore the relationship between the modulation period and dynamic responses of the LCVRs. Some of the results are shown in figure 7, in which the LCVRs exhibit different characteristics as the modulation period increases.

Combined with the characteristics of the divided region in the retardance shown in figure 5(a), it can be inferred that the state of LCMs is nearly perpendicular to the glass substrates at the beginning of each modulation cycle and will be reset by a falling edge signal as shown in figure 7(a). The entire process can be roughly divided into three stages according to the dynamic response characteristics:

(i) 20–80 ms: when the period of the applied voltage falls into this interval, the LCMs rotate from the stable region to the fast transit region shown in figure 5(c) under the falling edge signal. The LCMs rotate to the farthest position in fast transit region at a certain voltage when the inter-molecular force balanced the applied force. After then, as the driving voltage continues to increase, the inter-molecular force is smaller than the applied force, and the LCMs will return from the fast transit region to the stable region and enter the next modulation cycle.

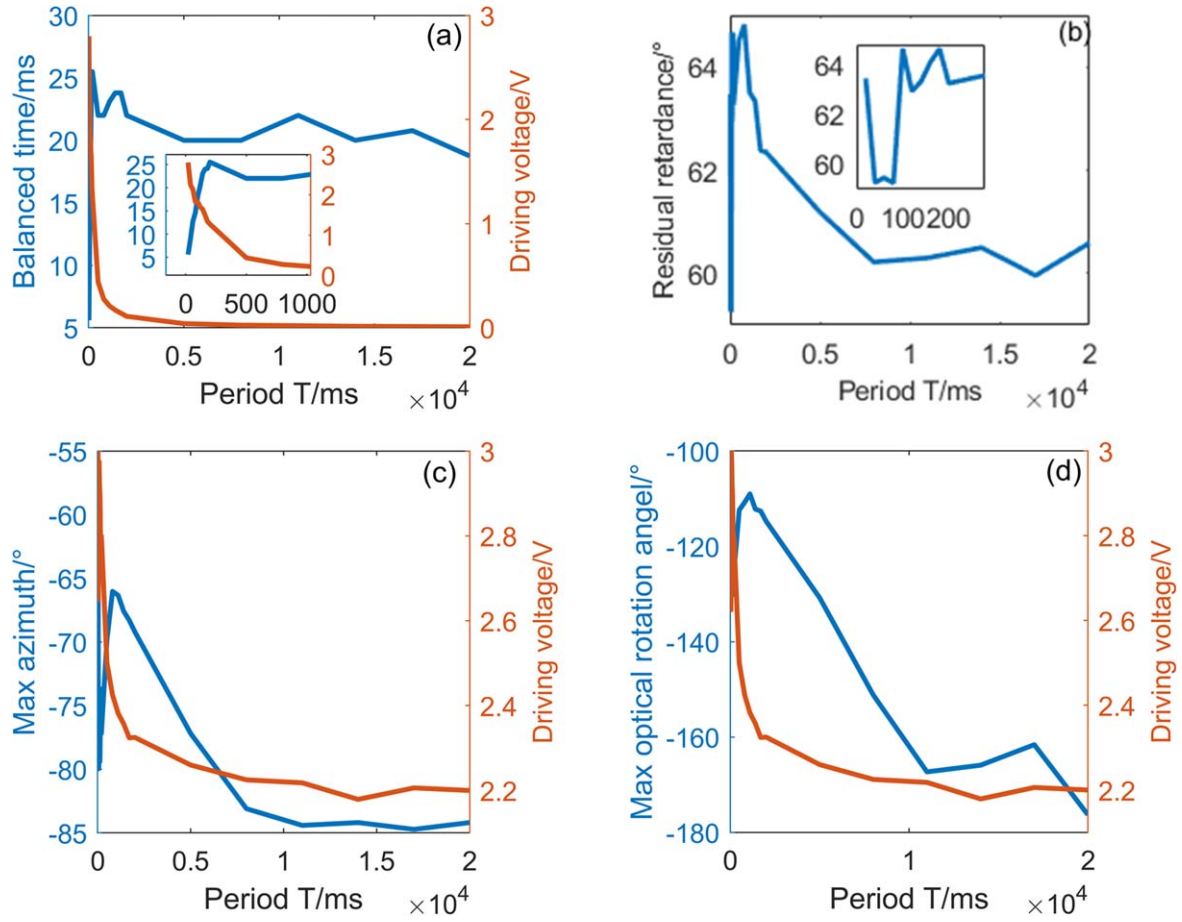

Figure 8. Relationships between (a) period and driving voltage as well as time when applied force balance inter-molecular force; (b) period and residual retardance; (c) period and maximum azimuth as well as corresponding voltage at maximum azimuth; (d) period and maximum optical rotation angle as well as corresponding voltage at maximum optical rotation angle.

(ii) 100–500 ms: a similar process like case (i) will happen to the LCMs. However, the LCMs have enough time to rotate from the stable region to the startup region and then back to the stable region as the modulation period increases.

(iii) 800–20000 ms: The LCMs behave similarly to the static modulation process. Under the falling edge signal, the state of the liquid crystal molecular achieves a complete reset gradually. They can rotate from stable region to the direction parallel to the *x*-axis and then back to the stable region when the modulation period is further increased.

Besides, we extract the driving voltage and the time when the applied force balances the intermolecular force according to the law of the variation of the retardance, as shown in figure 8(a). It can be observed that the required balance time increases sharply while the balance driving voltage decreases sharply when the modulation period is equivalent to the reset time. The required balance time stabilizes around 22 ms and the balance driving voltage stabilizes around 0 V when the modulation period exceeds 5000 ms. Therefore, the state reset time of the LCMs under the falling edge signal is about 22 ms, and the LCVRs exhibit the similar phase modulation properties as the static modulation processes when the modulation period is beyond 5000 ms. Meanwhile, we have also extract the residual retardance, as shown in figure 8(b). when the modulation period is less than 200 ms, the residual retardance fluctuates irregularly. It may be due to the measurement errors and unevenness caused by the flow of the liquid crystal. Since then, the residual retardance decreases slowly and finally stabilizes at around 60° which is slightly higher than residual retardance in the static modulation process, which indicates that the LCMs are not completely perpendicular to the glass substrates during dynamic modulation, and the LCMs will eventually get closer and closer to the *y*-axis. If a smaller residual retardance is required, a longer time at the high driving voltage should be maintained.

As shown in figures 7(b) and (c), it can be observed that the azimuth of the LCVRs fast axis changes with the driving voltage when the driving voltage is beyond the threshold. We usually define the long axis of the LCMs as the slow axis. Meanwhile, the long axis of the LCMs undergoes a process from parallel to the glass substrates to perpendicular to the glass substrates as the driving voltage increases, which is the reason why the azimuth has a voltage dependence. In order to analyze the relationship between azimuth and modulation period more clearly, we extract the maximum azimuth variation and corresponding voltage, as shown in figure 8(c). The voltage at the maximum azimuth variation gradually drops to 2.2 V, and the maximum azimuth

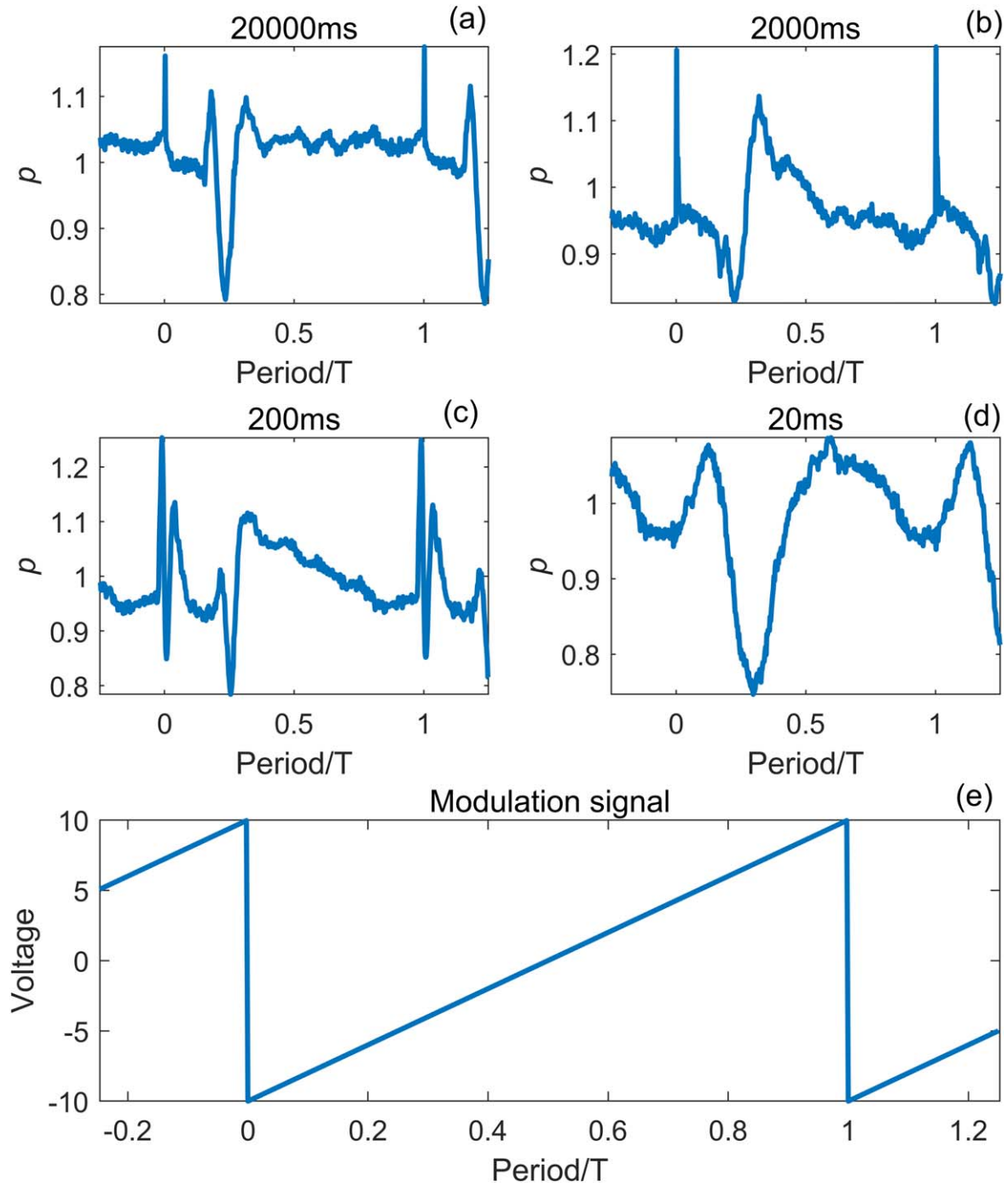

Figure 9. Degree of polarization p of the output light when the LCVRs is modulated by sawtooth signals of different periods of x ms (x =20–20 000). In order to more clearly and concisely show the evolution process, only the results of 20, 200, 2000, 20 000 ms are given in the figure.

gradually stabilizes around −84°. It can be inferred that the maximum azimuth appears at the fast transit region combined with the rotation process of the LCMs. Besides, we also have extracted the maximum optical rotation angle and voltage at maximum optical rotation angle to investigate the relationship between the CB properties and modulation period, as shown in figure 8(d). It can be observed that the voltage gradually stabilizes at 2.2 V, while the maximum optical rotation angle gradually decreases to −175°. It can be inferred that LCVRs exhibit strong CB properties when the LCMs are in the fast transit region, while the LCVRs show little CB properties when the LCMs are parallel or perpendicular to the glass substrates.

As shown in figure 7(d), it can be observed that the relative transmittance curve measured in dynamic modulation becomes more and more similar to the transmittance curve measured in static modulation. However, the variation of the relative transmittance at the driving voltage between 4 and 5 V deviates from the static measurement results. This may be caused by the fact that the optical elements in the FPMS have different transmittance for the different polarization states of the light.

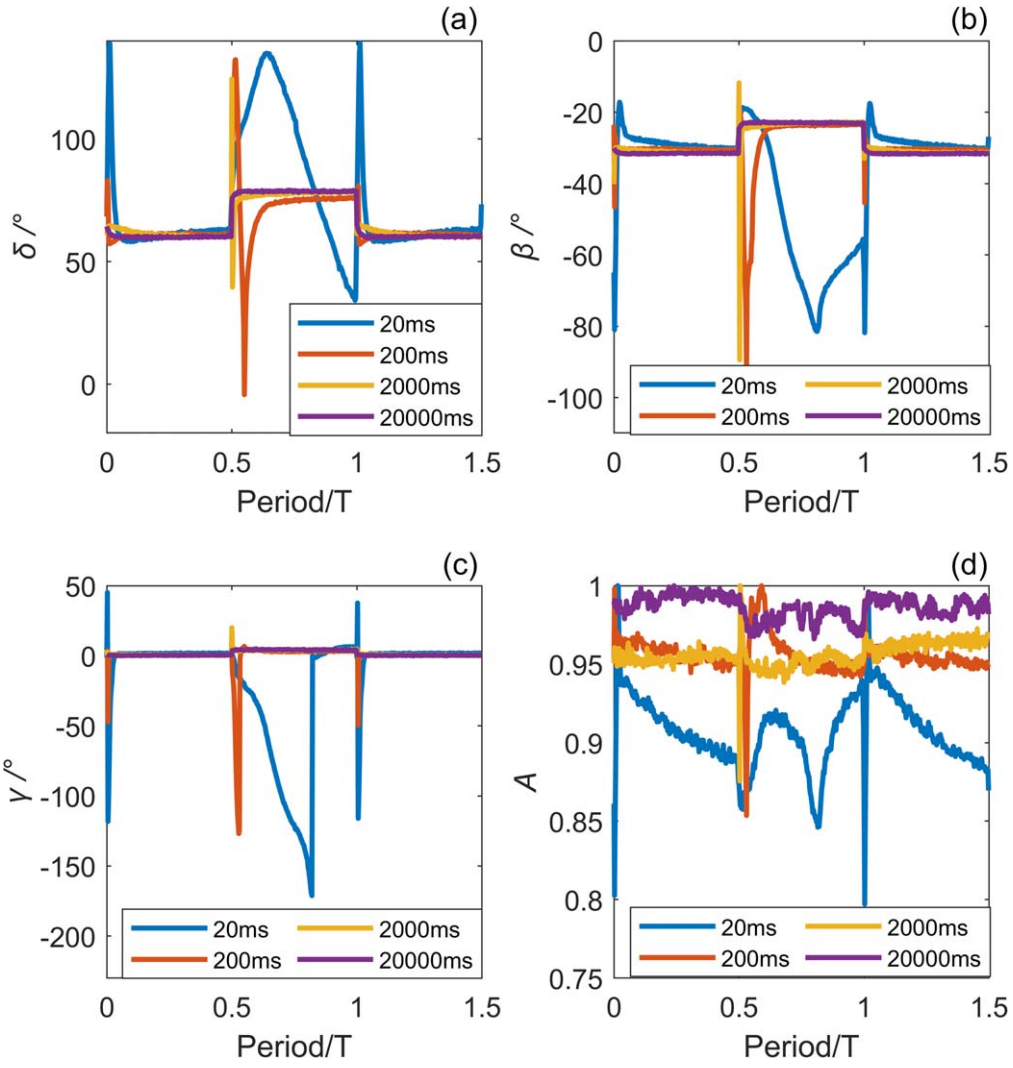

Figure 10. Optical parameters of the LCVRs modulated by square signals of different periods x ms (x = 20–20 000). In order to more clearly and concisely show the evolution process, only the results of 20, 200, 2000, 20 000 ms are shown in the figure.

In order to assess the depolarization of the LCVRs, the degree of the polarization p [41] of the output light can be defined by equation (8). Degree of polarization p of the output light when the LCVRs is modulated by sawtooth signals of different periods has been shown in figure 9. As can be seen, p of the output of the LCVRs varies with the driving voltage and the modulation period. We can observe a sharp fluctuation of p at 0 T in the modulation processes of 200, 2000 and 20 000 ms, but there is a smooth transition observed at 0 T in the modulation processes of 20 ms. Besides, there is a significant decrease in p between 0.18 and 0.3 T which corresponds to the process of the LCMs in the fast transit region. López-Téllez *et al* speculated that the drastic change in the retardance is the cause of the sharp fluctuation in p [23]. However, there is not a sudden change in the retardance between the 0.12 and 0.5 T, and the p fluctuates sharply in this interval in the modulation experiment of 20 ms. Meanwhile, when the LCMs is in the fast transit region or when the driving voltage changes rapidly, the states of the LCMs become unstable and change rapidly combined with the analysis of the extracted optical parameters in the sawtooth modulation experiments, causing drastic changes in the optical properties of the LCVRs. Therefore, it can be speculated that the fluctuation of the p is caused by the unstable and dramatic change of the LCMs states

$$p = \sqrt{\frac{S_1^2 + S_2^2 + S_3^2}{S_0^2}}. \tag{8}$$

4.2. Modulated by square signals with different amplitudes and periods

(i) Square wave signals with fixed amplitude and varying periods (z = 10 V, y = 20–2000 ms).

In this case, we will use the square wave signals with fixed amplitude of 10 V and vary the periods to study the relationship between the dynamic responsive characteristics and the modulation periods first. Some results of the achieved optical parameters are shown in figure 10.

It can be observed that the responses of the LCVRs at the falling or rising edges are changing with the modulation

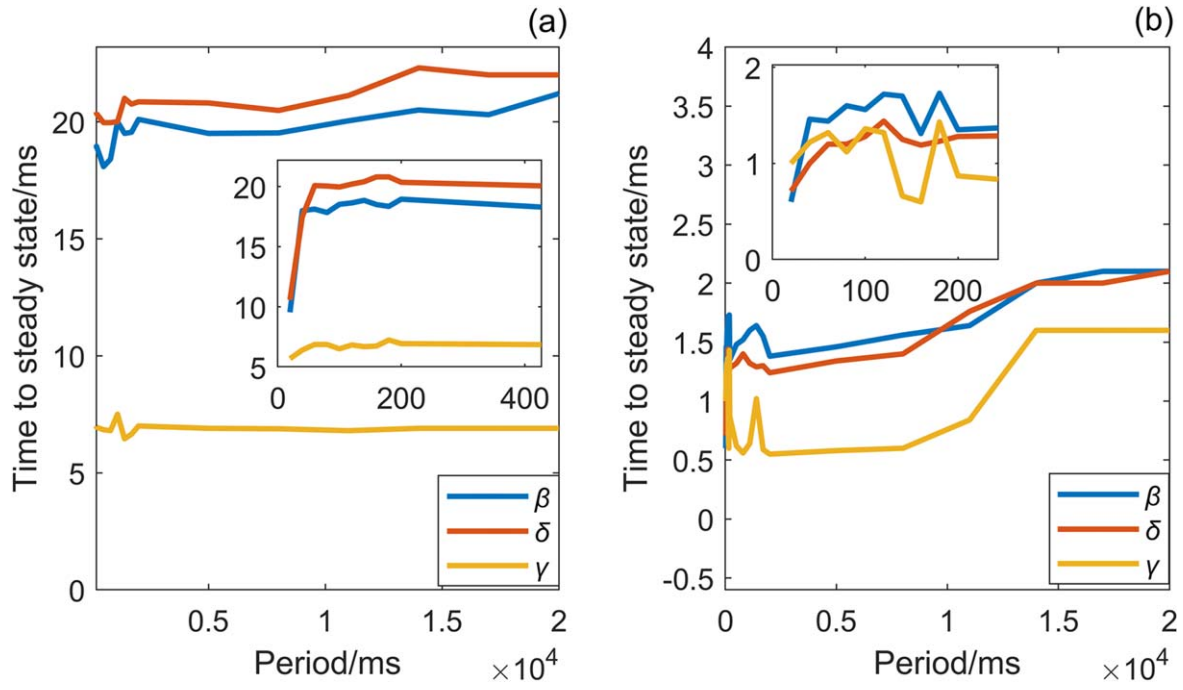

Figure 11. Response time of optical parameters at (a) falling edge and (b) rising edge of the square wave signal applied.

period. As shown in figure 10, the values of the retardance at 0.5 T and T are about 80° and 60° which are consistent with the results modulated by sawtooth wave signals. There is a difference of 8° between the values of azimuth at 0.5 and T, and the optical rotation angle at 0.5 and T is always around 0°. We can observe a relatively gradually stable modulation of the relative transmittance until the modulation period beyond 200 ms. However, it should be noted that the relative transmittance of the LCVRs is affected by that the optical elements in the FPMS, which may have different transmittance for the different polarization states of the light. Therefore, the analysis of relative transmittance is qualitative. Finally, the response time of the optical parameters at the falling edge is significantly larger than that at the rising edge. In order to more clearly observe the dynamic responsive characteristic of the optical parameters, we extract their response time at both the falling edge and rising edge of square wave signals, as shown in figure 11.

As shown in figure 11(a), at the falling edge, the response time of the azimuth is equivalent to the response time of the retardance, while it is much larger than the response time of the optical rotation angle. Besides, the response time of the azimuth increases before the 40 ms modulation period, and gradually stabilizes at about 20 ms. Meanwhile, the response time of the retardance increases before the 60 ms modulation period, and gradually stabilizes at about 22 ms. And the response time of optical rotation angle has been fluctuating around 7 ms. Then, at the rising edge, the response time of the optical parameters fluctuates before the 170 ms modulation period and then gradually increases. Finally, the response time of the azimuth, retardance and optical rotation angle are stable at 2.1 ms, 2 ms and 1.6 ms respectively, as shown in figure 11(b).

The degree of polarization p of the output light when the LCVRs is modulated by square signals of different periods of y ms (y = 20–20 000) has been shown in figure 12. The change of the p verifies the speculation from the sawtooth modulation experiments. The fluctuation of the p occurs at the transition point of the high and low driving voltage when the periods are 0.5 T and T, respectively, where the states of the LCMs are undergoing dramatic changes. Additionally, the slower fluctuation of p can be observed at the falling edge than at the rising edge, which is consistent with the result that the response time of the LCVRs under the falling edge is larger than that at the rising edge. It is not recommended to use signals with too short modulation period when using LCVRs for phase modulation, because a sharp state change of LCMs will result in a large change in p, which reduces measurement accuracy.

(ii) Square wave signals with different amplitudes and periods (z = 1–10, y = 20, 200, 2000).

Then the square wave modulated signals with different amplitudes (z = 1–10) when the periods are selected as y = 20, 200, and 2000 ms, are used to explore the relationship between the dynamic response characteristics and the driving voltage. It should be noted that the response characteristics of the LCVRs are stable when the modulation period is greater than 200 ms. So, the results of the period greater than 2000 ms are not given here.

(a) Modulation period of 2000 ms.

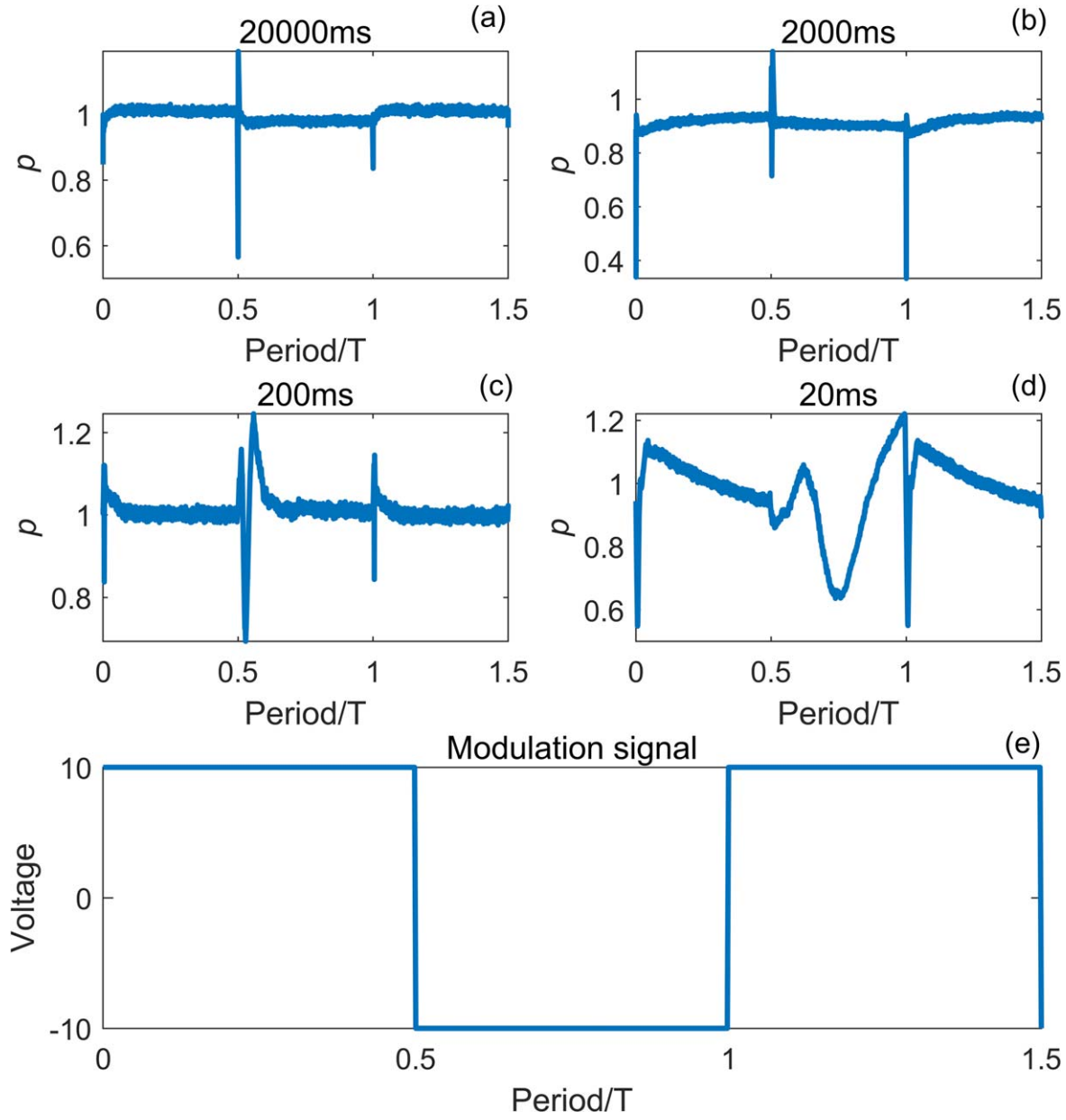

Figure 12. Degree of polarization of the output light when the LCVRs is modulated by square signals of different periods of y ms (y = 20–20 000). In order to more clearly and concisely show the evolution process, only the results of 20, 200, 2000, 20 000 ms are given in the figure.

Since the dynamic change of the driving voltage is slow when the modulation period is 2000 ms, the LCMs movement can keep up with the external loading without significant delay, the response time of the optical parameters at the edge of signal can be ignored, and the LCVRs have a relatively stable modulation state. The variation of the optical parameters at 0.5 T is consistent with the results in the sawtooth wave modulation experiment, and variation of the retardance and optical rotation angle at T remains the same as shown in figures 13(a) and (c), while the variation of the azimuth and the relative transmittance change with amplitude of the edge signals as shown in figures 13(b) and (d). It is observed that the transition process at the rising and falling edge varies with the amplitude of the signal. Therefore, we choose the data at the end of the signal to achieve a more stable modulation effect when a step modulation signal is used.

(b) Modulation period of 200 ms.

When the modulation period is 200 ms, due to the quick changes of the applied voltage, the LCMs rotation may lag behind the external loadings, therefore the response time of the optical parameters at the signal edge is non-ignorable, while the modulation of the LCVRs is considered being stabilized at the end of the signal edges. The variation of the optical parameters at 0.5 T is still consistent with the results in the sawtooth wave modulation experiment. Only the variation of the optical rotation angle at T remains the same as shown in figure 14(c), while the variations of the other optical

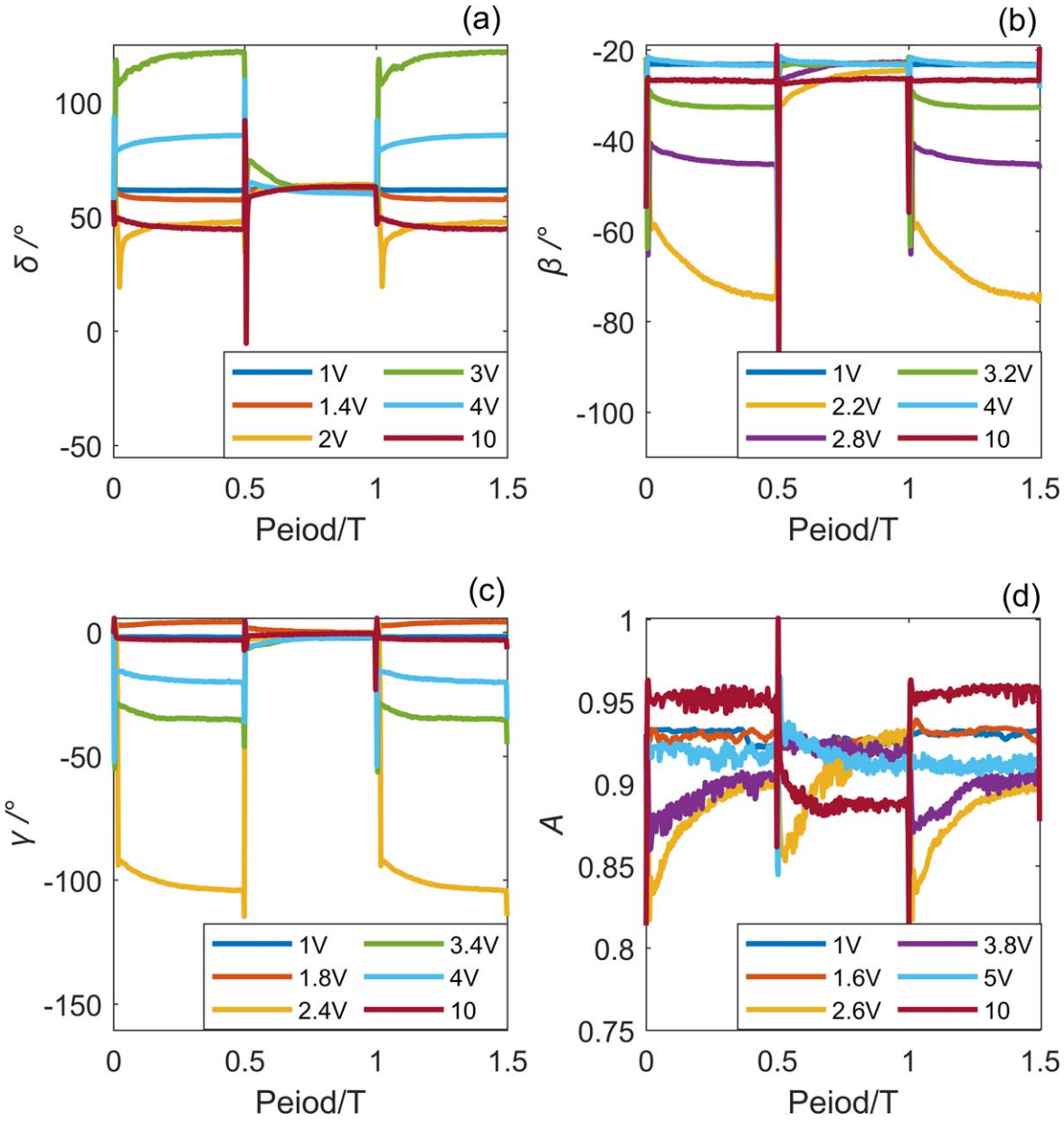

Figure 13. Optical parameters of the LCVRs modulated by a 0–z V (z = 1–10) square signals with a period of 2000 ms. In order to more clearly and concisely show the evolution process, only some important transition points are given.

parameters change with the amplitude of the edge signal irregularly as shown in figures 14(a), (b) and (d). It is observed that the transition process at the rising and falling edge cannot be ignored relative to the entire modulation processes.

(c) Modulation period of 20 ms.

Since the reaction of LCMs lag behind the driving voltage significantly, the response time of the optical parameters at the signal edge is approximately equivalent to the modulation period of 20 ms, thus, the change processes of the optical parameters are completely different from the cases when the modulation periods are 2000 and 200 ms. The variation of the optical parameters at T is complex and irregularly, while the variation of optical parameters at 0.5 T is roughly similar to the measurement results of the sawtooth wave modulation experiments, as shown in figure 15. It can be learned from the previous experimental results that the response time of the optical parameters at the falling edge is about 20 ms, and the response time is about 5 ms at the rising edge. However, there is only 10 ms left for the LCMs to reset the state. Therefore, the time for the LCMs to return to the predetermined position at the falling edge is insufficient, and the position that can be returned will be more and more deviated from the x-axis direction. Since the LCMs always have sufficient time to reach the predetermined position under the rising edge signal, the LCVRs have a relatively stable modulation state under the high voltage.

In order to more clearly observe the dynamic response characteristic of the optical parameters, we have extracted the dynamic response time of the retardance, azimuth and optical

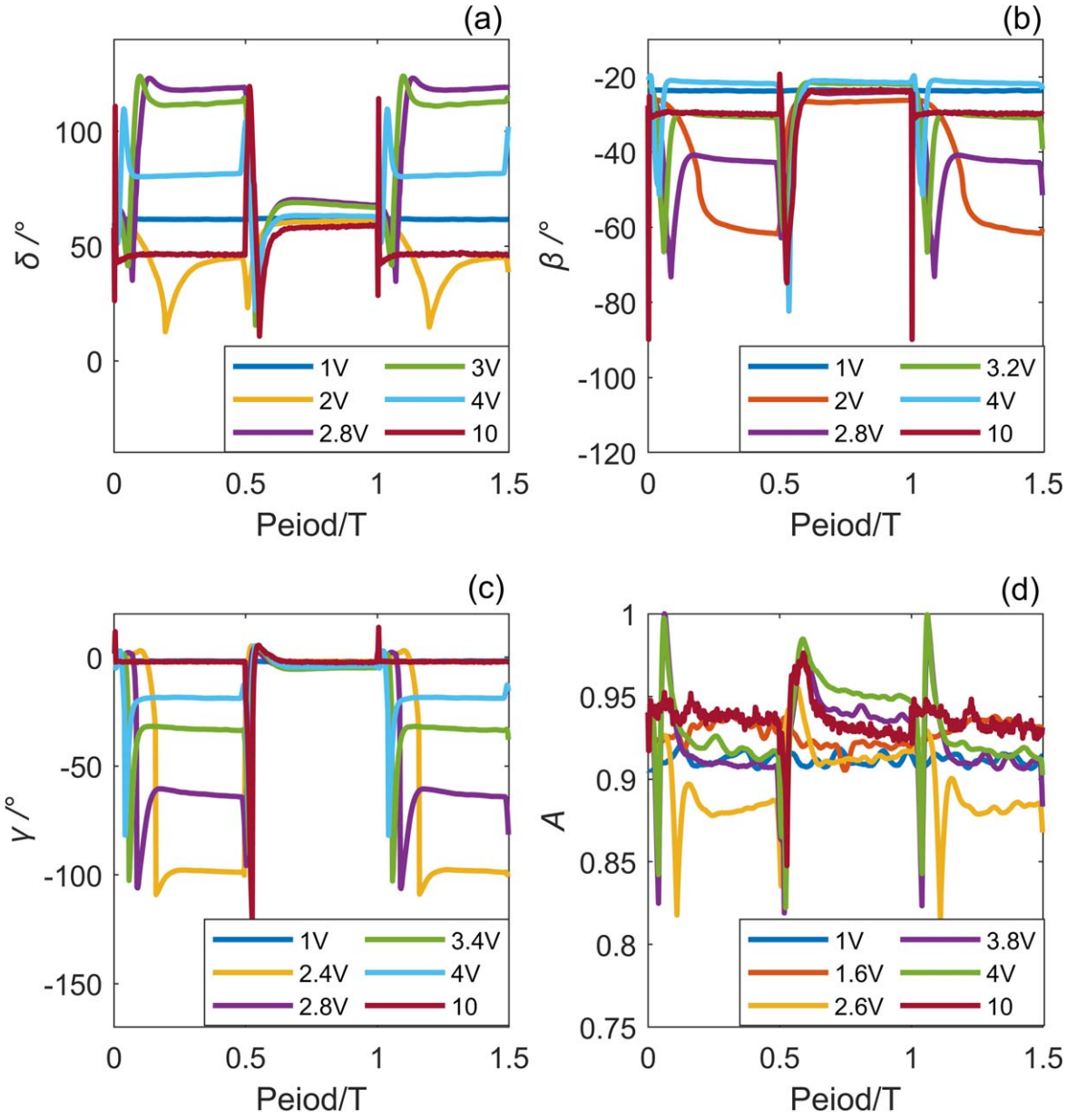

Figure 14. Optical parameters of the LCVRs modulated by a 0–z V (z = 1–10) square signals with a period of 200 ms. In order to more clearly and concisely show the evolution process, only some important transition points are given.

rotation angle at the falling edge and rising edge of when the amplitudes of the modulation signals are different, as shown in figure 16. According to the variation law of the extracted dynamic response time, we find the response time at the falling edge follows the variation law as equation (9), while the response time at the rising edge follows the variation law as equation (10), and the fitted parameters are listed in tables 1 and 2

$$T_{\mathrm{f}} = a_{\mathrm{f}} \exp(1 - b_{\mathrm{f}} V) + c_{\mathrm{f}}, \tag{9}$$

$$T_{\mathrm{r}} = a_{\mathrm{r}} \exp(b_{\mathrm{r}} V). \tag{10}$$

As shown in figure 16, the dynamic response times of the optical parameters at the signal edges are fitted well by the proposed empirical formula. Here, we define the voltage when the response time is no longer changing with amplitude of the edge signals as the voltage to the stead state V_{ts}, which is schematically shown in figures 16(a) and (b). The response time of the optical parameters at the falling edge increases as the driving voltage increases. When the driving voltage is beyond the V_{ts}, the response time gradually become steady. As shown in equation (9), the parameter a_{f}, b_{f}, and c_{f} determines the rising speed in the low amplitude region, the value of the V_{ts}, and the amplitude of the response time, respectively. As shown in table 1, the values of the parameter a_{f} should have been gradually reduced. However, the extracted response times has a large error due to the small variation of the optical parameters when the driving voltage is less than 2 V, which results in that the value of the a_{f} fluctuates with the increase of the modulation period. For the same reason, it is difficult to analyze the variation law of the V_{ts} from the value of the b_{f}. The variation of the c_{f} indicates that the response time of the azimuth and retardance in the 20 ms

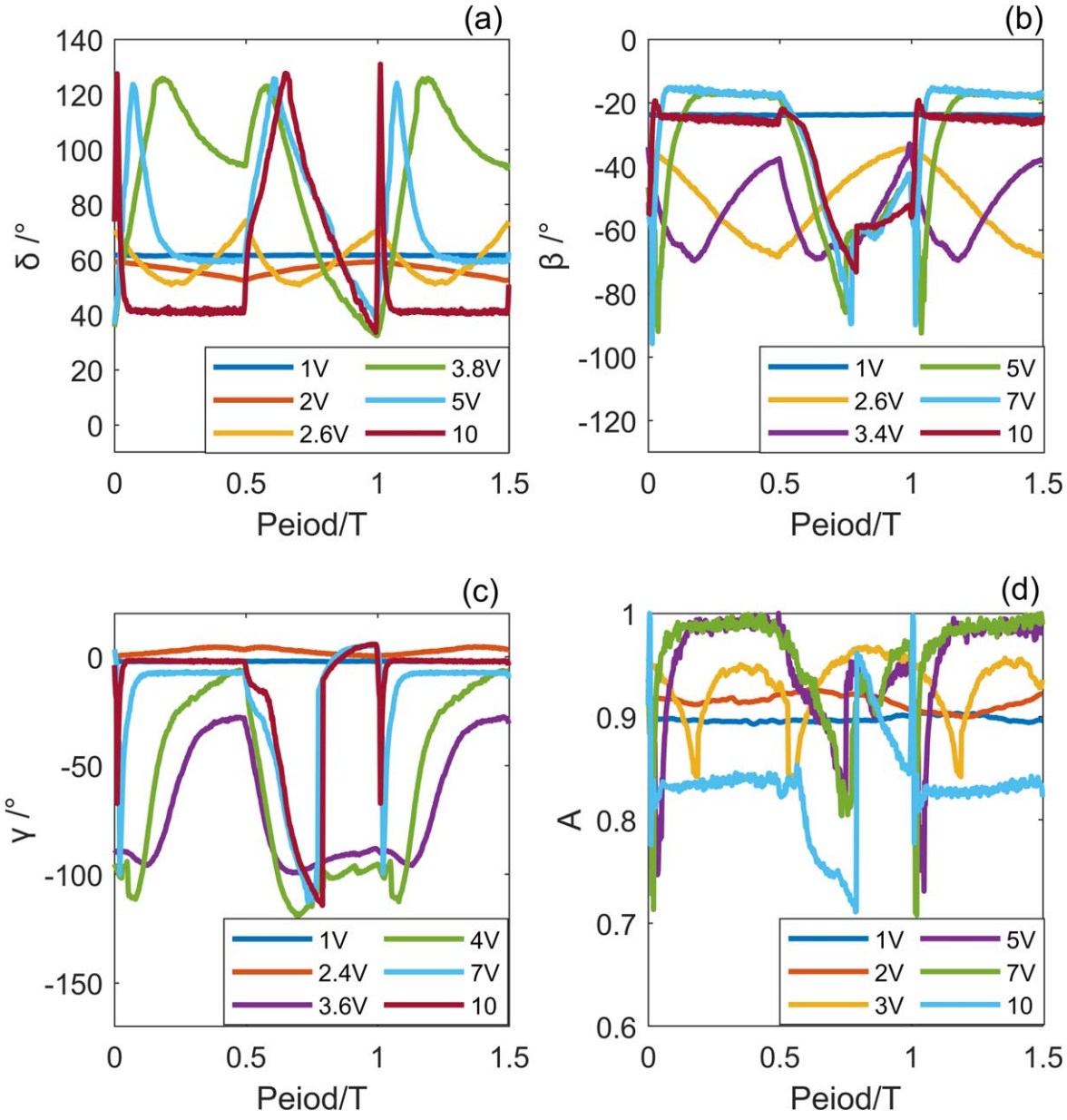

Figure 15. Optical parameters of the LCVRs modulated by a 0–z V (z = 1–10) square signals with a period of 200 ms. In order to more clearly and concisely show the evolution process, only some important transition points are given.

modulation period fluctuate around 8.8 and 8.5 ms which is different form the results 16 and 21 ms of the 200 and 2000 ms modulation period. However, the response time of the optical rotation angle fluctuates around 8 ms which is equivalent to that of the 200 and 2000 ms modulation period. The response time of the optical parameters at the signal rising edge decrease as the driving voltage increases. When the driving voltage is beyond the V_{ts}, the response time gradually stabilizes around the 0. As shown in equation (10), the parameter a_r determines the falling speed of the low amplitude region, and parameter b_r determines the value of V_{ts}. As shown in table 2, the values of the parameter a_r decreases and the values of the b_r increases as the modulation period increases. It corresponds to the phenomenon that the response time in the low amplitude region decreases more sharply and the value of the V_{ts} decreases as the modulation period increases.

Further, we extracted the retardance, azimuth and the optical rotation angle of the LCVRs at the time of 0.5 T and T when modulated by the square wave signals with different amplitudes, as shown in figure 17.

It is observed that the variations of the optical parameters at 0.5 T in the 200 and 2000 ms modulation periods are consistent with the results in the sawtooth wave modulation experiment. Also, the variations of the azimuth in the range of 2–3.6 V are not 0°, while the optical rotation angles in the range of the 2.2–5 V are not 0°. It indicates the existence of CB property in this interval. The maximum variation azimuth is about 45° when the amplitude of the applied voltage is 2.2 V. Meanwhile, the maximum optical rotation angle is

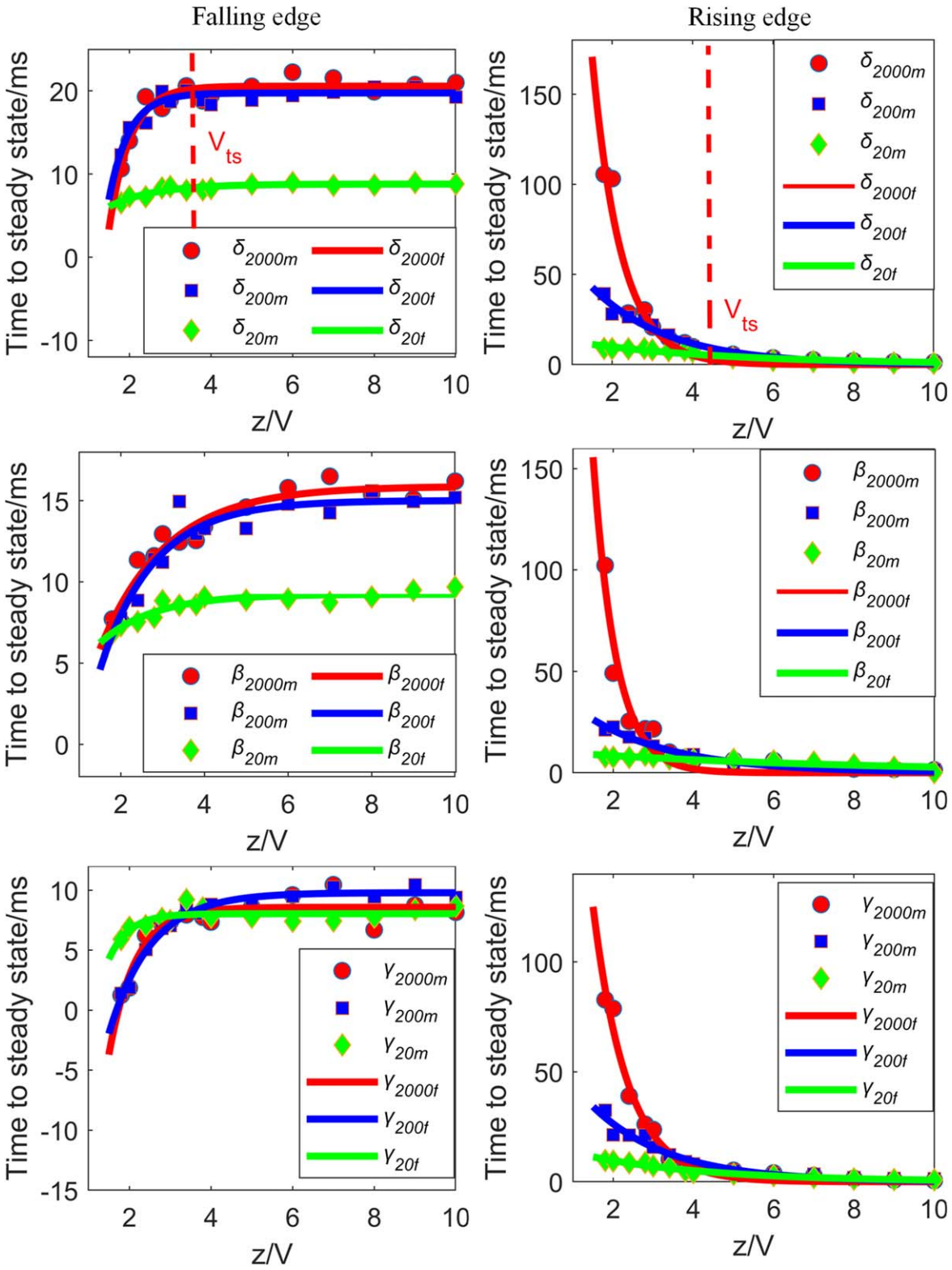

Figure 16. Response time of the optical parameters under falling edge and rising edge of square wave signal of different amplitude. Subscripts '*m*' represent the results extracted from the measured optical parameters, and the subscripts '*f*' represent the results fitted by the proposed empirical formula.

about -100° when the amplitude of the applied voltage is 2.4 V. We can learn from the results in the sawtooth modulation experiments that the LCMs are in the fast transit region in the driving voltage range of 2–3 V. The state of the LCMs in this region change rapidly, causing the azimuth and the optical rotation angle to change drastically within the driving voltage region. However, due to the different characteristics of LB and CB, the states of the LCMs at the

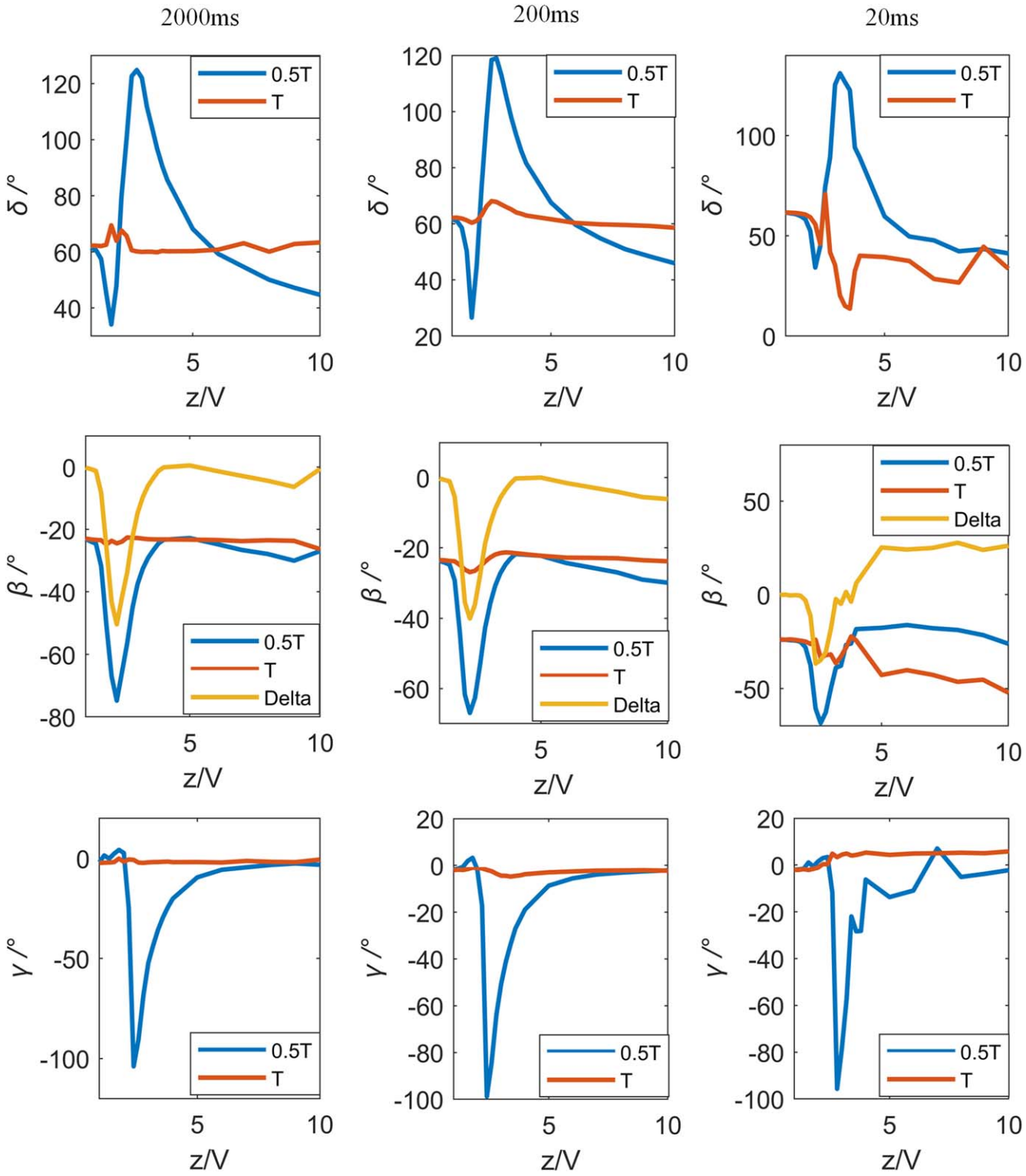

Figure 17. Optical parameters of LCVRs at 0.5 T, T under square wave signal with different amplitude: delta represents the difference of the optical parameters at 0.5 T and T.

maximum azimuth variation and maximum optical rotation angle are different, which results in different driving voltages for them. As for the results of the 20 ms modulation period, the values of the optical parameters at 0.5 T are similar to the results of the sawtooth wave modulation experiments in general. However, the values of the optical parameters at T fluctuate dramatically with the amplitude of the edge signal. This is because the response time of the falling edge signal is much larger than that of the rising edge signal, and the LCMs have enough time to reach the predetermined modulation state of the driving voltage at 0.5 T, while there is insufficient time for the LCMs to return to the state of the driving voltage at T.

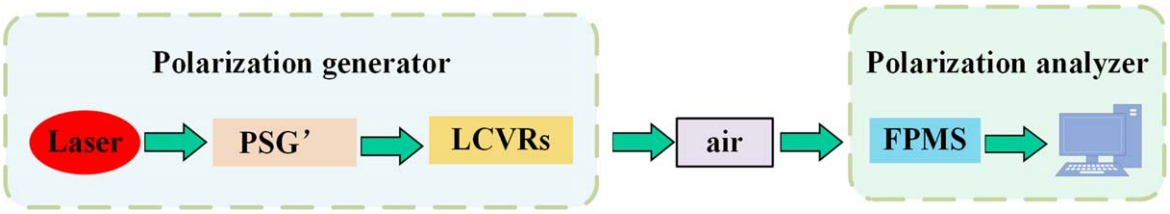

Figure 18. Schematic diagram of air mull matrix measurement experiment: the new polarization generator is consisted by the old polarization generator and the LCVRs, and the air is the sample.

Table 1. Fitting results of the falling edge signals.

Period	2000 ms			200 ms			20 ms		
Fit parameters	β	δ	γ	β	δ	γ	β	δ	γ
a_f	−9.575	−115.2	−45.23	−12.26	−95.02	−18.66	−3.503	−3.857	−28.58
b_f	0.6343	1.933	1.536	0.776	2.001	0.9749	0.7694	0.9011	2.013
c_f	15.89	20.57	8.571	15.01	19.749	9.79	9.233	8.797	8.037

Table 2. Fitting results of the rising edge signals.

Period	2000 ms			200 ms			20 ms		
Fit parameters	β	δ	γ	β	δ	γ	β	δ	γ
a_r	2168	1391	733.3	51.86	93.78	74.53	11.06	16.6	18.29
b_r	−1.756	−1.398	−1.179	−0.4538	−0.5213	−0.5199	−0.1364	−0.2635	−0.3217

So, it is not recommended to use a step signal with high amplitude for modulation in the use of the LCVRs when the modulation period is less than 200 ms.

4.3. Reconstruction of air Mueller matrix based on dynamic characteristics of LCVRs

In order to verify the achieved dynamic characteristics of LCVRs, we suppose the LCVRs as polarization modulation devices in our optical system as schematically shown in figure 18, and try to measure the Mueller matrix of the air, in which the sawtooth signal with period of 200 ms modulation period have been used to modulate the LCVR. Additionally, a comparison between the Mueller matrices of air measured with the proposed and conventional characterization methods has been carried out. The Mueller matrix of the air and the corresponding average residual errors of Muller matrix elements obtained with the proposed and conventional characterization method are shown as equation (11)

$$\mathbf{M}_{\mathrm{air\_}p} = \begin{bmatrix} 1.0100 & -0.0091 & 0.0100 & -0.0098 \\ -0.0097 & 1.0069 & -0.0092 & 0.0083 \\ -0.0099 & 0.0066 & 0.9902 & 0.0084 \\ 0.0099 & -0.0082 & 0.0097 & 0.9907 \end{bmatrix},$$
$$\mathrm{Er}_{\mathrm{ave\_}p} = 0.0091, \tag{11-1}$$

$$\mathbf{M}_{\mathrm{air\_}c} = \begin{bmatrix} 1.0603 & -0.0082 & -0.0812 & 0.0001 \\ 0.0115 & 1.0684 & 0.0313 & 0.0608 \\ -0.0052 & 0.0896 & 0.9938 & 0.0568 \\ 0.0648 & -0.0099 & 0.0543 & 1.0069 \end{bmatrix},$$
$$\mathrm{Er}_{\mathrm{ave\_}c} = 0.0490, \tag{11-2}$$

where, $\mathbf{M}_{\mathrm{air\_}p}$ and $\mathrm{Er}_{\mathrm{ave\_}p}$ represents the Muller matrices and average residual errors of Muller matrix elements obtained with proposed characterization method, $\mathbf{M}_{\mathrm{air\_}c}$ and $\mathrm{Er}_{\mathrm{ave\_}c}$ represents the Muller matrices and average residual errors of Muller matrix elements obtained with conventional characterization method.

The average error of the Mueller matrix obtained with the proposed method is less than 1% based on the theoretical Mueller matrix of the air, while the average error of the matrix obtained with conventional method is 4.90%. To a certain extent, the results demonstrate the effectiveness and advantages of the dynamic characterization procedure of the LCVRs.

5. Conclusions

A method based on the Mueller matrix has been proposed to characterize the LCVRs, with which the LCVRs can be described by the optical parameters such as the retardance, azimuth, relative transmittance and optical rotation angle. The improvement of the proposed method is shown by the 15 times reduced residual errors of the Mueller matrices

compared with conventional characterization methods. Through several typical dynamic measurement experiments using a high-speed Stokes polarimeter, we demonstrated the driving-voltage-dependence of these optical parameters as well as the existence of both LB and CB properties in the LCVRs modulation processes. Then we have obtained the continuous modulation characteristics and step response characteristics of LCVRs by analyzing the extracted optical parameters. Based on the analysis of the extracted optical parameters, we have established the relationship between the modulation characteristics and the rotation state of the LCMs by combining the measured responses to continuous and step modulation signals. An empirical formula is given to describe the relationship between the response time and amplitude of the square wave modulation signal as well. Finally, Mueller matrix of the air reconstructed based on the achieved dynamic characteristics of LCVRs and the corresponding average residual errors less than 1% further demonstrates the validity of the proposed method.

Acknowledgments

This work was funded by the National Natural Science Foundation of China (Grant No. 51575214, 51525502, 51727809, and 51805193); the National Key Research and Development Plan (Grant No. 2017YFF0204705); the Natural Science Foundation of Hubei Province of China (Grant No. 2018CFA057); and the National Science and Technology Major Project of China (Grant No. 2017ZX02101006-004).

ORCID iDs

Hao Jiang https://orcid.org/0000-0003-0561-5058
Xiuguo Chen https://orcid.org/0000-0002-7067-5084
Shiyuan Liu https://orcid.org/0000-0002-0756-1439

References

[1] Liu C-C, Ren D-Q, Zhu Y-T, Dou J-P and Guo J 2016 A high-contrast imaging polarimeter with a stepped-transmission filter based coronagraph *Res. Astron. Astrophys.* **16** 073
[2] Collins P, Kyne G, Lara D, Redfern M, Shearer A and Sheehan B 2013 The Galway astronomical Stokes polarimeter: an all-Stokes optical polarimeter with ultra-high time resolution *Exp. Astron.* **36** 479–503
[3] Bagnulo S, Belskaya I, Cellino A and Kolokolova L 2017 Polarimetry of small bodies and satellites of our solar system *Eur. Phys. J. Plus* **132** 405
[4] Elmore D F, Lites B W, Tomczyk S, Skumanich A, Dunn R B, Schuenke J A, Streander K V, Leach T W, Chambellan C and Hull H K 1992 Advanced Stokes polarimeter: a new instrument for solar magnetic field research *Proc. SPIE* **1746** 22–34
[5] Ottaviani M, Chowdhary J and Cairns B 2019 Remote sensing of the ocean surface refractive index via short-wave infrared polarimetry *Remote Sens. Environ.* **221** 14–23
[6] Tyo J S, Goldstein D L, Chenault D B and Shaw J A 2006 Review of passive imaging polarimetry for remote sensing applications *Appl. Opt.* **45** 5453–69
[7] Howe J D, Miller M A, Blumer R V, Petty T E, Stevens M A, Teale D M and Smith M H 2000 Polarization sensing for target acquisition and mine detection *Proc. SPIE* **4133** 202–14
[8] Guo X, Wood M and Vitkin A I 2006 Angular measurements of light scattered by turbid chiral media using linear Stokes polarimeter *J. Biomed. Opt.* **11** 041105
[9] Samim M, Krouglov S, James D F and Barzda V 2016 Characterization of heterogeneous media using nonlinear Stokes–Mueller polarimetry *J. Opt. Soc. Am.* B **33** 2617–25
[10] Tan Y, Zhang S and Zhang Y 2009 Laser feedback interferometry based on phase difference of orthogonally polarized lights in external birefringence cavity *Opt. Express* **17** 13939–45
[11] Tan Y, Wang W, Xu C and Zhang S 2013 Laser confocal feedback tomography and nano-step height measurement *Sci. Rep.* **3** 2971
[12] Gladish J C and Duncan D D 2014 Alignment and temperature effects in liquid-crystal-based active polarimetry *Appl. Opt.* **53** 3982–92
[13] Goudail F, Terrier P, Takakura Y, Bigué L, Galland F and DeVlaminck V 2004 Target detection with a liquid-crystal-based passive Stokes polarimeter *Appl. Opt.* **43** 274–82
[14] Zhang Y, Zhao H, Song P, Shi S, Xu W and Liang X 2014 Ground-based full-sky imaging polarimeter based on liquid crystal variable retarders *Opt. Express* **22** 8749–64
[15] Nagaraju K, Phanindra D, Prasad S K, Rao D S and Sreekumar P 2018 Full Stokes polarimetry using dual-frequency liquid crystals *Proc. SPIE* **10702** 107024X
[16] López-Téllez J and Bruce N 2014 Mueller-matrix polarimeter using analysis of the nonlinear voltage–retardance relationship for liquid-crystal variable retarders *Appl. Opt.* **53** 5359–66
[17] Pust N J and Shaw J A 2006 Dual-field imaging polarimeter using liquid crystal variable retarders *Appl. Opt.* **45** 5470–8
[18] Wei P, Gu H, Chen X, Jiang H, Zhang C and Liu S 2019 Characterization of a liquid crystal variable retarder by Mueller matrix ellipsometry *Proc. SPIE* **11053** 110531Q
[19] Bueno J M 2000 Polarimetry using liquid-crystal variable retarders: theory and calibration *J. Opt.* A **2** 216
[20] Hilfiker J, Herzinger C, Wagner T, Marino A, Delgais G and Abbate G 2004 Mueller-matrix characterization of liquid crystals *Thin Solid Films* **455** 591–5
[21] Hu D, Liu Q, Yu L, Zhu Y and Song L 2015 LCVR phase retardation characteristic calibration method based on SVM regression *Int. Conf. Optoelectronics and Microelectronics (ICOM)* vol 45 *(16–18 July 2015)*
[22] Terrier P, Charbois J-M and Devlaminck V 2010 Fast-axis orientation dependence on driving voltage for a Stokes polarimeter based on concrete liquid-crystal variable retarders *Appl. Opt.* **49** 4278–83
[23] López-Téllez J M, Bruce N C and Rodríguez-Herrera O G 2016 Characterization of optical polarization properties for liquid crystal-based retarders *Appl. Opt.* **55** 6025–33
[24] Heredero R, Uribe-Patarroyo N, Belenguer T, Ramos G, Sánchez A, Reina M, Pillet V M and Álvarez-Herrero A 2007 Liquid-crystal variable retarders for aerospace polarimetry applications *Appl. Opt.* **46** 689–98
[25] Ma J, Xu C and Yao Y 2017 Real-time observation of liquid crystal molecular directions based on a snapshot polarimeter *Chin. Opt. Lett.* **15** 061601
[26] Kowa H, Muraki K, Tsukiji M, Takayanagi A and Umeda N 1996 Simultaneous measurement of linear and circular birefringence with heterodyne interferometry *Proc. SPIE* **2873** 29–32
[27] Yan K, Guo Q, Wu F, Sun J, Zhao H and Kwok H-S 2019 Polarization-independent nematic liquid crystal phase

modulator based on optical compensation with sub-millisecond response *Opt. Express* **27** 9925–32
[28] Gandorfer A M 1999 Ferroelectric retarders as an alternative to piezoelastic modulators for use in solar Stokes vector polarimetry *Opt. Eng.* **38** 1402–9
[29] Imazawa R, Kawano Y, Ono T and Itami K 2016 Development of real-time rotating waveplate Stokes polarimeter using multi-order retardation for ITER poloidal polarimeter *Rev. Sci. Instrum.* **87** 013503
[30] Zhang S, Gu H, Liu J, Jiang H, Chen X, Zhang C and Liu S 2018 Characterization of beam splitters in the calibration of a six-channel Stokes polarimeter *J. Opt.* **20** 125606
[31] Liu J, Zhang C, Zhong Z, Gu H, Chen X, Jiang H and Liu S 2018 Measurement configuration optimization for dynamic metrology using Stokes polarimetry *Meas. Sci. Technol.* **29** 054010
[32] López-Téllez J and Bruce N 2013 Experimental method to characterize a liquid-crystal variable retarder and its application in a Stokes polarimeter *Proc. SPIE* **8785** 87852J
[33] Konforti N, Marom E and Wu S-T 1988 Phase-only modulation with twisted nematic liquid-crystal spatial light modulators *Opt. Lett.* **13** 251–3
[34] Yeh P and Gu C 2010 *Optics of Liquid Crystal Displays* vol 67 (New York: Wiley) pp 75–85
[35] Wang B and Oakberg T C 1999 A new instrument for measuring both the magnitude and angle of low level linear birefringence *Rev. Sci. Instrum.* **70** 3847–54
[36] Lo Y-L 2012 Extraction of effective parameters of turbid media utilizing the Mueller matrix approach: study of glucose sensing *J. Biomed. Opt.* **17** 097002
[37] Manhas S, Swami M, Buddhiwant P, Ghosh N, Gupta P and Singh K 2006 Mueller matrix approach for determination of optical rotation in chiral turbid media in backscattering geometry *Opt. Express* **14** 190–202
[38] López-Téllez J and Bruce N 2014 Stokes polarimetry using analysis of the nonlinear voltage-retardance relationship for liquid-crystal variable retarders *Rev. Sci. Instrum.* **85** 033104
[39] Baba J S and Boudreaux P R 2007 Wavelength, temperature, and voltage dependent calibration of a nematic liquid crystal multispectral polarization generating device *Appl. Opt.* **46** 5539–44
[40] Rodríguez-Nuñez O, López-Téllez J M, Rodríguez-Herrera O G and Bruce N C 2017 Calibration and data extraction in nonoptimized Mueller matrix polarimeters *Appl. Opt.* **56** 4398–405
[41] Firdous S and Ikram M 2007 Stokes polarimetry for the characterization of bio-materials using liquid crystal variable retarders *Proc. SPIE* **6632** 66320F